Mitochondrial carrier protein overloading and misfolding induce aggresomes and proteostatic adaptations in the cytosol

Yaxin Liu[a,†], Xiaowen Wang[a,†], Liam P. Coyne[a,†], Yuan Yang[a,‡], Yue Qi[b], Frank A. Middleton[c], and Xin Jie Chen[a,c,*]

[a]Department of Biochemistry and Molecular Biology, [b]Department of Pathology, and [c]Department of Neuroscience and Physiology, State University of New York Upstate Medical University, Syracuse, NY 13210

ABSTRACT **Previous studies in yeast showed that mitochondrial stressors not directly targeting the protein import machinery can cause mitochondrial precursor overaccumulation stress (mPOS) in the cytosol independent of bioenergetics. Here, we demonstrate mPOS and stress responses in human cells. We show that overloading of mitochondrial membrane carrier, but not matrix proteins, is sufficient to induce cytosolic aggresomes and apoptosis. The aggresomes appear to triage unimported mitochondrial proteins. Interestingly, expression of highly unstable mutant variants of the mitochondrial carrier protein, Ant1, also induces aggresomes despite a greater than 20-fold reduction in protein level compared to wild type. Thus, overloading of the protein import machinery, rather than protein accumulation, is critical for aggresome induction. The data suggest that the import of mitochondrial proteins is saturable and that the cytosol is limited in degrading unimported mitochondrial proteins. In addition, we found that *EGR1*, eEF1α, and ubiquitin C are up-regulated by Ant1 overloading. These proteins are known to promote autophagy, protein targeting to aggresomes, and the processing of protein aggregates, respectively. Finally, we found that overexpression of the misfolded variants of Ant1 induces additional cytosolic responses including proteasomal activation. In summary, our work captured a profound effect of unimported mitochondrial proteins on cytosolic proteostasis and revealed multiple anti-mPOS mechanisms in human cells.**

Monitoring Editor
Thomas D. Fox
Cornell University

Received: Jan 23, 2019
Revised: Mar 11, 2019
Accepted: Mar 15, 2019

INTRODUCTION

Mitochondria are semiautonomous organelles that contain more than 1000 polypeptides (Calvo *et al.*, 2016). Only 13 of these proteins are encoded by mitochondrial DNA (mtDNA) and synthesized in the mitochondrial matrix. The remaining ~99% of mitochondrial proteins are nuclear encoded and are synthesized in and imported from the cytosol (Chacinska *et al.*, 2009). Effective biogenesis of mitochondria requires the coordinated expression of proteins from both the cytosolic and the mitochondrial protein synthesis machineries. For example, respiratory enzymes of the oxidative phosphorylation (OXPHOS) pathway are large protein complexes on the inner mitochondrial membrane (IMM) that require the coordinated expression of subunits from both mtDNA and nuclear DNA (Richter-Dennerlein *et al.*, 2016). Decreased import of specific OXPHOS components into mitochondria is generally expected to affect ATP production and energy homeostasis in the cell. Moreover, a global defect in protein import would be expected to affect mitochondrial biogenesis and reduce cell viability, as mitochondria carry out essential cellular functions in addition to ATP production (Wang, 2001; Shadel and Horvath, 2015; Gottschling and Nystrom, 2017). Several human diseases have been found to be caused by mutations in genes encoding the core mitochondrial protein import machinery (Koehler *et al.*, 1999; Kang *et al.*, 2017; Vukotic *et al.*, 2017).

This article was published online ahead of print in MBoC in Press (http://www.molbiolcell.org/cgi/doi/10.1091/mbc.E19-01-0046) on March 20, 2019.

†These authors contributed equally to this work.

‡Present address: Department of Psychiatry, Tongji Hospital, Tongji Medical College, Huazhong University of Science and Technology, Wuhan, Hubei 430030, China.

*Address correspondence to: Xin Jie Chen (chenx@upstate.edu).

Abbreviations used: Ant1, isoform 1 of adenine nucleotide translocase; AV, autophagic vacuole; CCCP, cyanide *m*-chlorophenyl hydrazine; CMV, cytomegalovirus; IMM, inner mitochondrial membrane; IMS, intermembrane space; mPOS, mitochondrial precursor overaccumulation stress; OMM, outer mitochondrial membrane; OXPHOS, oxidative phosphorylation; PI, propidium iodide.

However, despite the expected consequences of reduced import noted above, how reduced import may cause diseases is not fully understood.

Our previous studies have indicated that severe proteostatic stress in mitochondria can reduce protein import. This kills cells by a mechanism independent of bioenergetics, termed mitochondrial precursor overaccumulation stress (mPOS), which is characterized by the toxic accumulation of unimported mitochondrial proteins in the cytosol (Wang and Chen, 2015). In yeast, we showed that misfolded variants of Aac2, the homologue of human Ant1 involved in ATP/ADP exchange across the IMM, causes proteostatic stress in the membrane and destabilizes multiple protein complexes including the TIM22 and TIM23 protein translocases (Liu *et al.*, 2015). This reduces protein import and leads to the accumulation of unimported proteins in the cytosol. This is sufficient to cause lethal cytosolic proteostatic stress before the reduced protein import causes defects in critical mitochondrial functions. Given that protein import efficiency can be affected by many conditions such as IMM stress and low membrane potential, it was speculated that various mitochondrial stressors may contribute to diseases via mPOS, in addition to their effect on bioenergetic output (Coyne and Chen, 2018).

It is unknown whether unimported mitochondrial protein can accumulate in the cytosol and induce mPOS in human cells, and if so, whether adaptive mechanisms exist to tolerate and suppress the stress. In the current study, we found that overexpression of mitochondrial carrier proteins, including Ant1, is sufficient to induce the formation of large cytosolic aggresomes that appear to contain unimported mitochondrial proteins. The data suggest that the mitochondrial protein import pathway is saturable, that the cytosol has a limited capacity to degrade unimported proteins, and that aggresome formation is a defense mechanism against mPOS. These findings are clinically relevant as overexpression of Ant1 has been observed in several human diseases (Sylven *et al.*, 1993; Dorner *et al.*, 1997; Dorner and Schultheiss, 2000; Gabellini *et al.*, 2002; Laoudj-Chenivesse *et al.*, 2005; Kriaucionis *et al.*, 2006; Forlani *et al.*, 2010). We also found that overexpression of pathogenic misfolded variants of Ant1 induces additional proteostatic responses in the cytosol. The results support the idea that mitochondrial protein overloading and misfolding have severe consequences on cytosolic proteostasis, and that multiple mechanisms exist to protect mammalian cells against the resulting mPOS.

RESULTS

Overloading of mitochondrial carrier proteins induces the formation of cytosolic aggresomes

We attempted to induce mPOS in mammalian cells by overexpressing a select panel of nuclear genes encoding mitochondrial proteins from the cytomegalovirus (CMV) promoter in human embryonic kidney 293T (HEK293T) cells. We reasoned that protein overloading may saturate the import machinery and, consequently, lead to the accumulation and aggregation of unimported mitochondrial proteins in the cytosol (i.e., mPOS). To detect potential cytosolic protein aggregates, we used fluorescence microscopy after staining transfected cells with an aggresome dye that specifically recognizes protein aggregates. Aggresomes can be effectively induced by inhibiting the proteasome with MG132 (Figure 1, A and B). We overexpressed mitochondrial matrix proteins including aconitase (Aco2), isoform 2 of isocitrate dehydrogenase (Idh2), and succinate dehydrogenase subunit A (SdhA). We found that *IDH2* and *SDHA* do not induce detectable aggresomes, and that

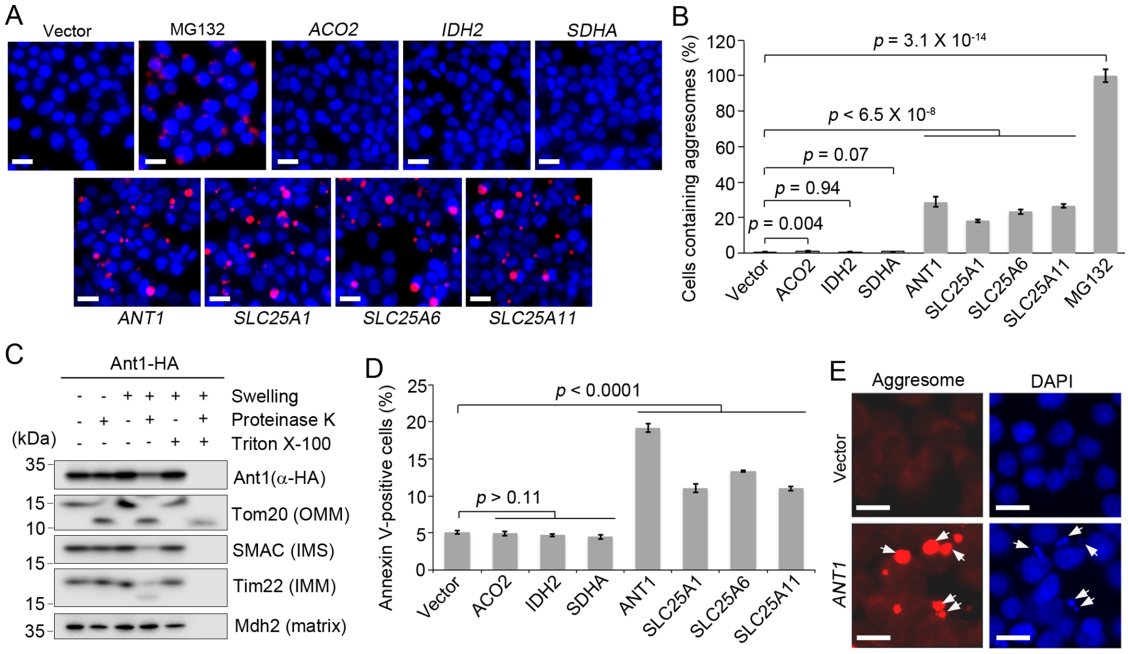

FIGURE 1: Overexpression of mitochondrial carrier proteins induces cytosolic aggresome formation and apoptotic cell death. (A) Fluorescence microscopy showing the induction of aggresomes by overexpression of *ANT1* (or *SLC25A4*), *SLC25A1*, *SLC25A6*, and *SLC25A11*, but not of *ACO2*, *IDH2*, and *SDHA*. MG132 was used as a positive control for aggresome induction. Scale bars, 20 μm. (B) Quantitation of aggresome formation in A, normalized to the number of nuclei stained by DAPI. Error bars represent SEM of 16 fields of scanning from two independent transfections with a total of 12,000–28,000 cells examined. (C) Submitochondrial localization of Ant1-HA. (D) Annexin V-positive and propidium iodide negative early apoptotic HEK293T cells overexpressing the mitochondrial proteins as indicated. Error bars are SEM of three independent experiments. (E) Staining of *ANT1*-transfected HEK293T cells with aggresome dye and DAPI. Arrows denote micronuclei that colocalize with aggresomes. Scale bars, 20 μm.

ACO2 overexpression only marginally increased aggresome formation. Interestingly, overexpression of several mitochondrial carrier proteins drastically induced the formation of distinct structures in the cytosol that are intensely stained by the aggresome dye (Figure 1, A and B). These proteins include isoform 1 (Ant1 or Slc25A4) and 3 (Ant3 or Slc25A6) of adenine nucleotide translocase, the citrate transporter (Slc25A1), and the 2-oxoglutarate/malate carrier (Slc25A11). When entering mitochondria, the transfected carrier proteins appear to be targeted to the IMM, as exemplified by submitochondrial localization experiments in cells transfected with *ANT1-HA* (Figure 1C). HEK293T cells predominantly express *ANT2* and *ANT3*, while *ANT1* is expressed at very low levels. RNA-Seq analysis (see below) showed that the mRNA level of *ANT1* in the transfected cells is 3.71-fold higher than the sum of the endogenously expressed *ANT2* and *ANT3*. These observations suggest that the mitochondrial import pathway is saturable in vivo. Expectedly, a threshold level of carrier overexpression appears to be required for the detection of aggresome induction. When transfected in HeLa cells, the *CMV-ANT1* construct is expressed approximately 1.7-fold lower compared with HEK293T cells (Supplemental Figure 1A). No significant induction of aggresomes was observed. Similarly, the two misfolded variants of Ant1 (see below) also failed to induce aggresome formation in HeLa cells (Supplemental Figure 1B).

We found that the frequency of aggresome formation correlates with increased early apoptotic cells (annexin V-positive, propidium iodide [PI]–negative; Figure 1D) and total apoptotic cells (total annexin V-positive cells; Supplemental Figure 1C) 24 h posttransfection. Extranuclear puncta positive to DAPI (4′, 6-diamidino-2-phenylindole) staining colocalize with the aggresomes in *ANT1*-overexpressing cells (Figure 1E). These DNA structures likely represent fragmented chromatins that are commonly detected in the cytosol of apoptotic cells. These findings suggest that mitochondrial carrier overloading is sufficient to induce mPOS and cell death. The rate of apoptosis is not further increased 36 or 48 h posttransfection and, correspondingly, there is no decrease in the ~50% of cells that are nonapoptotic (double-negative cells; Supplemental Figure 1D). In conjunction with our observed ~70% transfection efficiency, this supports the idea that while many transfected cells do indeed die, others are able to mount effective cellular defense mechanisms to remain viable.

We then determined whether acute inhibition of mitochondrial protein import can also induce aggresome formation. Interestingly, we found that sublethal concentrations of MitoBloCK-6 (Supplemental Figure 2A; Dabir *et al.*, 2013), which inhibits protein import, only marginally induce aggresome formation (Supplemental Figure 2B). Sublethal concentrations of carbonyl cyanide *m*-chlorophenyl hydrazine (CCCP; Supplemental Figure 2C), which uncouples the IMM, do not induce aggresome formation (Supplemental Figure 2D). These compounds would be expected to globally inhibit mitochondrial biogenesis. Thus, it is possible that severe defects in mitochondria-associated function(s) prevent aggresome formation, even though protein import is directly or indirectly inhibited.

Aggresomes induced by mitochondrial carrier proteins contain densely packed protein aggregates and may triage unimported mitochondrial proteins

Using transmission electron microscopy, we confirmed the presence of large structures with dense materials resembling protein aggresomes (Ags) in cells transfected with an *ANT1*-expressing plasmid (Figure 2A(ii)), but not with the empty vector (Figure 2A(i)). These aggresomes appear to have a much higher electron density compared with classic cytosolic aggresomes (Garcia-Mata *et al.*, 1999; Kolodziejska *et al.*, 2005). In contrast to classic aggresomes that are membrane-free (Kopito, 2000), we observed double- or single-membrane structures enclosing some, but not all *ANT1*-induced aggresomes (Figure 2A, (iii) and (iv)). The membranes may be derived from phagophores via the process of autophagy. Areas of low electron density were detected within some aggresomes (Figure 2A(iv)), which could result from lysosomal clearance of intra-aggresomal protein aggregates as the final step in the process of aggrephagy. Autophagic/lysosomal clearance of intact aggresomes

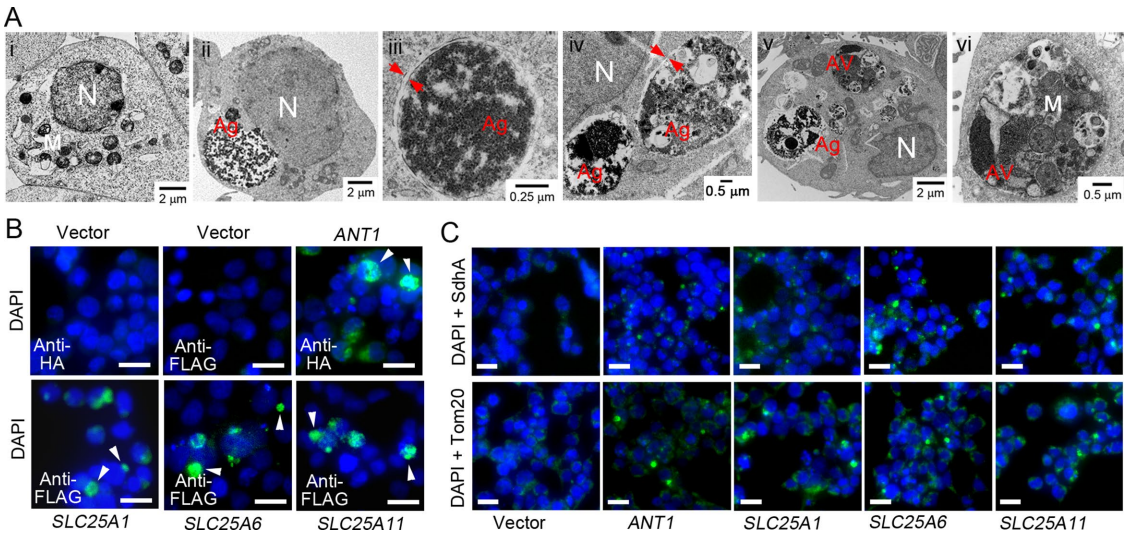

FIGURE 2: Aggresomes (Ags) and autophagic vacuoles (AVs) induced by overexpression of mitochondrial carriers in HEK293T cells. (A) Transmission electron microscopy. i, cells transfected with the control vector. ii–vi, *ANT1*-transfected cells. N, nucleus; M, mitochondria. Red arrows in iii and iv indicate membranes. (B) Immunostaining showing the condensation of HA- and FLAG-tagged mitochondrial carriers in the aggresome-like cytosolic vesicles. Scale bars, 20 μm. (C) Immunostaining showing the presence of mitochondrial proteins SdhA and Tom20 in cytosolic vesicles in cells overexpressing mitochondrial carrier proteins. Scale bars, 20 μm.

seems highly unlikely due to their large size. We speculate that the giant aggresomes arise when aggregate deposition exceeds the capacity of lysosomal clearance, leading to the recruitment and continuous expansion of the phagophore membrane to sequester proteins.

In addition to aggresomes that contain mainly aggregated proteins, *ANT1* overexpression also induced large structures resembling autophagic vacuoles (AVs) that harbor a mixture of protein aggregates, membrane vesicles, and mitochondria (Figure 2a, (v) and (vi)). However, while the AVs appear to stain positively for LC3 by fluorescence microscopy (see Supplemental Figure 8C), we did not see an overall increase in the LC3-II to LC3-I ratio in *ANT1*-transfected cells (Supplemental Figure 8A).

We speculated that the cytosolic aggresomes and AVs may contain triaged mitochondrial proteins that fail to enter the mitochondria. Unfortunately, the broad emission spectrum of the aggresome dye precluded a direct colocalization of unimported mitochondrial proteins and the aggresomes. However, we detected strong immunofluorescence signals of the hemagglutinin (HA)-tagged Ant1, and the FLAG-tagged Slc25A1, Slc25A6, and SlcA25A11, in vesicular structures resembling aggresomes and AVs (Figure 2B). Furthermore, we found that the endogenously expressed mitochondrial proteins SdhA and Tom20 are also condensed in large spherical vesicles in cells overexpressing the mitochondrial carrier proteins (Figure 2C). Taken together, these data support the idea that the cytosolic aggresomes and AVs are induced to triage the overexpressed mitochondrial carrier proteins, as well as endogenous mitochondrial proteins. The latter may have failed to enter mitochondria because of a competition for binding to import receptors with the overloaded proteins.

ANT1 overexpression activates the expression of the nuclear transcriptional factor Egr1 without severely affecting oxidative phosphorylation

Next, we determined the effect of *ANT1* overexpression on mitochondria. We found that the size of mitochondria in *ANT1* overexpressing cells is not drastically changed compared with control cells (Figure 3A). More importantly, no protein aggregates were detected inside mitochondria in aggresome-forming cells. *ANT1* overexpression causes moderate but significant reductions in basal and maximal respiratory rates (Figure 3, B–D), and respiratory coupling efficiency appears unaffected (Figure 3E). The steady-state levels of representative subunits of respiratory complexes and the mitochondrial matrix protein Aco2 are unchanged in total cell lysates, but are moderately reduced in isolated mitochondria (Figure 3F). This suggests distribution of these proteins to extramitochondrial compartments because of ineffective import.

To learn the mechanism by which Ant1 overloading induces aggresome formation in the cytosol, we first examined the nuclear transcriptome in *ANT1*-overexpressing cells. RNA-Seq revealed that, despite the drastic proteostatic reconfiguration in the cytosol as manifested by aggresome formation, *ANT1* overexpression affected the transcription of only a limited number of nuclear genes (Figure 3, G and H, and Supplemental Table 1). No genes involved in oxidative phosphorylation, bioenergetic adaptation, or the classic heat shock response are up-regulated. Instead, we found that *EGR1* (early growth response gene-1) is the most up-regulated gene, although the magnitude of up-regulation is moderate. *EGR1* encodes a transcriptional factor with diverse cellular functions including cell proliferation and stress response. It was recently shown to play a central role in the regulation of autophagy (Peeters *et al.*, 2019).

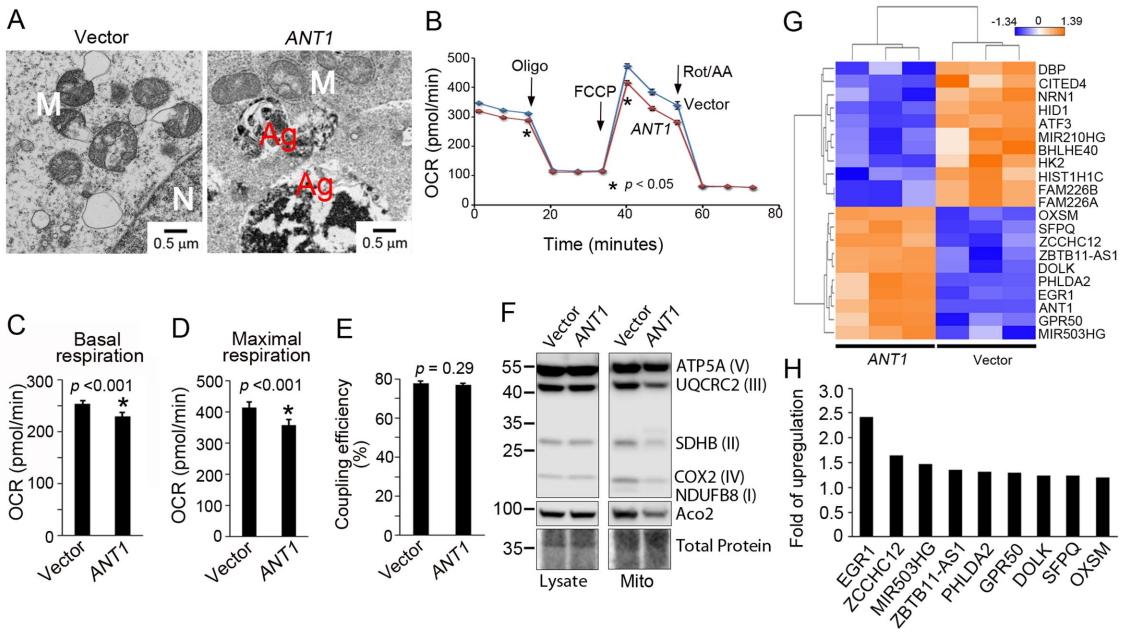

FIGURE 3: *ANT1* overexpression has only moderate effects on oxidative phosphorylation and the nuclear transcriptome. (A) Transmission electron microscopy showing mitochondrial structure in aggresome-forming cells expressing *ANT1*. Ag, aggresome; M, mitochondria; N, nucleus. (B–E) Oxygen consumption rates (OCRs) and coupling efficiency of transfected HEK293T cells, determined by Seahorse XF96e extracellular flux analyzer with sequential injections of oligomycin (Oligo), carbonylcyanide-4-trifluoromethoxyphenylhydrazone (FCCP), and rotenone/antimycin A (Rot/AA). Six independent transfections were performed. Error bars indicate standard deviations. Coupling efficiency (E) is defined by the ratio between ATP production–driven respiration rate and basal respiration rate. (F) Western blot showing the levels of representative mitochondrial proteins in total cell lysates and isolated mitochondria from *ANT1*-transfected cells. (G) Heatmap of differentially expressed genes in cells transfected by *ANT1* vs. control vector. (H) Genes up-regulated by *ANT1* overexpression.

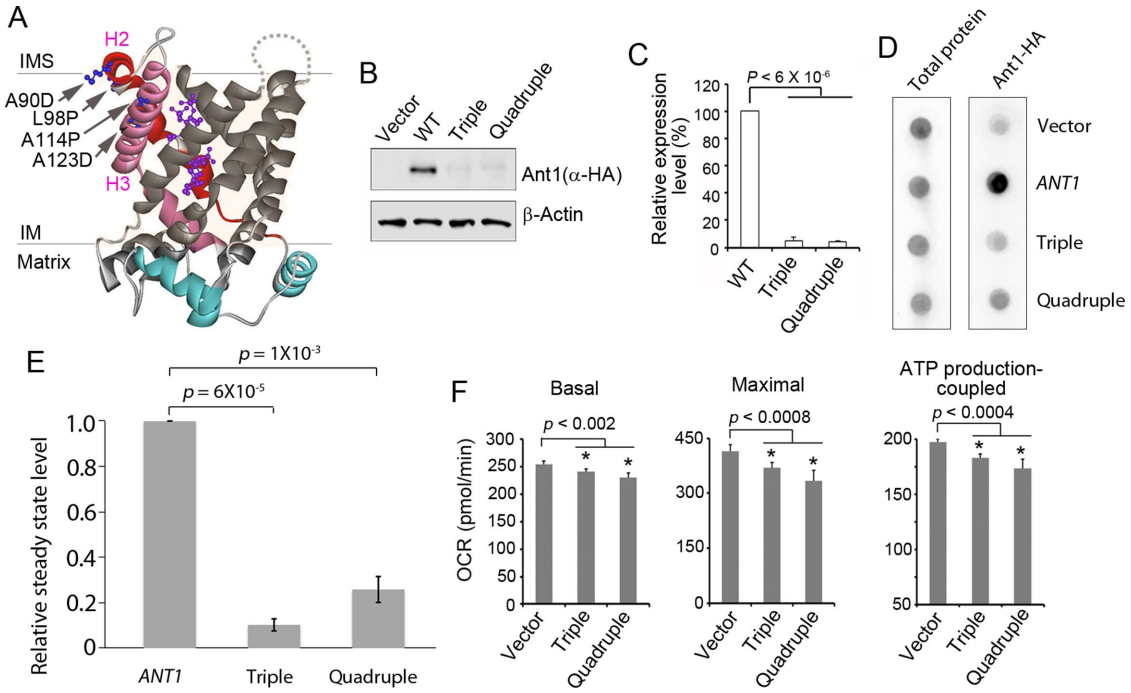

FIGURE 4: Stability and bioenergetic effect of misfolded Ant1. (A) Crystal structure of the yeast Aac2 protein (Ruprecht *et al.*, 2014). The amino acids equivalent to those mutated in human *ANT1* are denoted by arrows. Carboxylatractyloside in magenta indicates the putative nucleotide binding site. H2, α-helix 2; H3, α-helix 3; IM, inner membrane; IMS, intermembrane space. (B) Western blot analysis showing the steady-state levels of the triple and quadruple mutants of Ant1 in HEK293T cells. (C) Quantitation of the protein levels in B ($n = 3$). Error bars represent SD. (D) Dot blot analysis showing the levels of the triple and quadruple mutants of Ant1 relative to the wild type. Transfected cells were sonicated in lysis buffer with 5% SDS plus 8 M urea, and the total lysates were directly spotted to the membrane without centrifugation. Protein signals were detected with an anti-HA antibody. (E) Quantitation of dot blot signals in D. Error bars represent SEM from four replicates. (F) Oxygen consumption rate of transfected HEK293T cells as measured by Seahorse extracellular flux analyzer. The basal respiration, maximal respiration, and ATP production–driven respiration were calculated. Error bars indicate standard deviations.

Among the seven protein-coding genes up-regulated by *ANT1*, predicted *EGR1* target genes are highly overrepresented (*Z*-score 18.7) and include *ZCCHC12* (zinc finger CCHC-type containing 12, or Sizn1), *PHLDA2*, *SFPQ*, and *DOLK* (Supplemental Table 2). It is possible that these genes participate in the Egr1-orchestrated autophagic program to facilitate aggresome formation to triage unimported mitochondrial proteins.

Induction of aggresome formation in the cytosol by Ant1 is independent of Ant1 accumulation

One interpretation of the data presented above is that aggresomes are induced simply by the cytosolic accumulation of hydrophobic carrier proteins, such as Ant1. However, here we demonstrate that Ant1 overexpression can induce aggresome formation without substantial protein accumulation. We did so by taking advantage of mutant Ant1 variants that accumulate poorly in HEK293T cells.

Our previous studies in yeast showed that mPOS can be induced by various conditions that directly or indirectly affect protein import, including the expression of a misfolded variant of Aac2, the orthologue of human Ant1 (Wang and Chen, 2015). We then asked how human cells might respond to stress induced by the expression of misfolded Ant1. We generated variants of Ant1 that contain multiple misfolding mutations. These mutations include A90D, L98P, A114P, and A123D that are known to cause pathologies including autosomal-dominant progressive external ophthalmoplegia, bipolar affective disorder, dementia, myopathy, and cardiomyopathy (Kaukonen *et al.*, 1999, 2000; Napoli *et al.*, 2001; Siciliano *et al.*, 2003; Deschauer *et al.*, 2005; Palmieri *et al.*, 2005; Simoncini *et al.*, 2017). These mutations occur on α-helices 2 and 3 in the proximity of IMM-intermembrane space interface (Figure 4A), with some of them causing the protein itself to aggregate on the IMM (Liu *et al.*, 2015). Consistent with this, we found that the steady-state levels of the triple ($Ant1^{A90D,L98P,A114P}$) and quadruple ($Ant1^{A90D,L98P,A114P,A123D}$) mutants of Ant1 are reduced to only 4.77% ($p = 5.89 \times 10^{-6}$, unpaired Student's *t* test) and 4.06% ($p = 3.98 \times 10^{-7}$, unpaired Student's *t* test) of the wild-type Ant1 level, respectively (Figure 4, B and C). Meanwhile, detectable mRNA levels of the mutant *ANT1* variants were equivalent to that of wild type as determined by RNA-Seq. Such a low accumulation suggests that these mutations cause increased turnover of the proteins either on or before reaching the IMM. Another interpretation is that the mutations cause the mutant proteins to aggregate, thus reducing the solubility in RIPA buffer and compromising detection by Western blotting. To test this, we attempted to enhance extraction of the quadruple mutant with various harsh detergents and chaotropic agents. This did not substantially increase protein recovery as shown by Western blot analysis (Supplemental Figure 3). Moreover, direct dot blot analysis of precleared lysates confirmed the low-level accumulation of the mutant Ant1 in the transfected cells (Figure 4, D and E). Clearly, the mutant proteins accumulate at very low levels compared with the wild-type Ant1. Using a Seahorse metabolic flux analyzer, we found that expression of the triple and quadruple mutants of Ant1 have only moderate effects on mitochondrial respiration and respiratory coupling efficiency (Figure 4F).

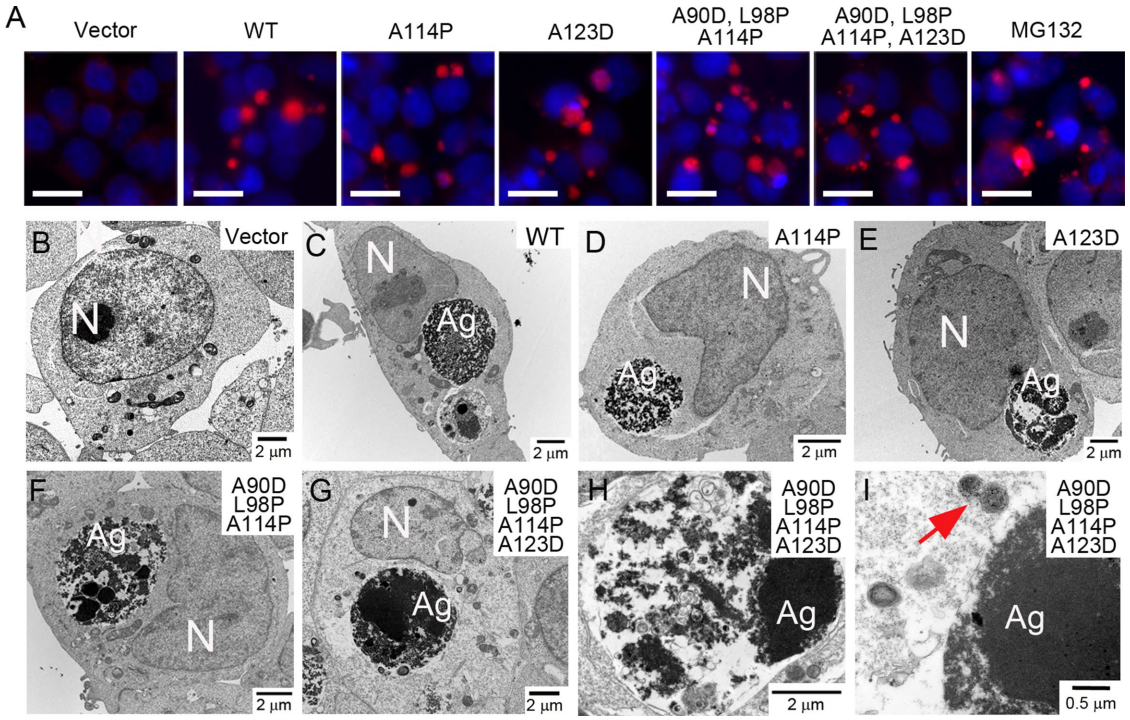

FIGURE 5: Induction of aggresomes by mutant Ant1. (A) Staining of transfected HEK293T cells with an aggresome dye showing the induction of aggresomes. MG132 treatment was used as a positive control. Scale bars, 20 μm. (B–I) Transmission electron microscopy of HEK293T cells transfected with vector (B), the wild-type *ANT1* (C), $ant1^{A114P}$ (D), $ant1^{A123D}$ (E), $ant1^{A90D,L98P,A114P}$ (F), and $ant1^{A90D,L98P,A114P,A123D}$ (G–I). N, nucleus; Ag, aggresome; H, a representative aggresome that contains small vesicles; I, aggresome–cytosol interface. Arrow denotes membrane-rich vesicles in the vicinity of an aggresome that contains electron-dense particles resembling aggregated proteins.

Despite drastically reduced steady-state levels of the misfolded triple ($Ant1^{A90D,L98P,A114P}$) and quadruple ($Ant1^{A90D,L98P,A114P,A123D}$) mutant variants of Ant1, aggresome induction remains substantial (Figure 5A). We note that the A123D mutation affects the function of respiratory complexes (Ogunbona *et al.*, 2018) and completely inactivates adenine nucleotide transport activity (Palmieri *et al.*, 2005). Aggresome induction by the quadruple mutant, which has the A123D mutation, is therefore independent of nucleotide transport. Examination by electron microscopy revealed that aggresomes induced by the mutant Ant1 are morphologically indistinguishable from those induced by the wild-type *ANT1* (Figure 5, B–G). Small vesicles were frequently seen within the aggresomes (Figure 5H). Membrane-rich vesicles containing dark punctates were detected in the vicinity of the aggresomes (Figure 5I). Similar structures have been observed in flies when the mitochondrial protein import machinery is directly knocked down (Liu *et al.*, 2018). We speculate that these vesicles may be involved in the delivery of aggregated proteins to the aggresomes in the HEK293T cells.

Expression of mutant Ant1 activates additional proteostatic pathways in the cytosol

In a search for extra effects of mutant compared with wild-type Ant1, we examined apoptosis and mitochondrial membrane potential. We found that the triple and quadruple mutants of Ant1 do not further increase apoptosis when compared with the wild-type protein (Figure 6A), consistent with a comparable subpopulation of cells with severely depolarized mitochondria (Supplemental Figure 4). Expression of the mutant Ant1 moderately increases rather than decreasing the relative mitochondrial membrane potential in the main subpopulation of the cells that maintain their potential (Figure 6B), which suggests a preferential effect on processes that utilize (e.g., ATP synthesis) rather than generate (e.g., the electron transport chain) the potential.

To uncover additional cytosolic pathways induced by mutant Ant1, we performed RNA-Seq analysis on cells expressing the triple and quadruple mutant Ant1. Interestingly, this revealed that the triple and quadruple mutants alter the expression of 206 and 560 genes, respectively (Figure 6C and Supplemental Tables 3 and 4), far more than observed for wild-type Ant1. Thirty-two genes were commonly up-regulated by the two mutants (Figure 6D and Supplemental Figure 5, A and B). Like the cells overexpressing the wild-type *ANT1* (Figure 3H), expression of *EGR1*, *ZCCHC12*, and *SFPQ* is activated by the triple and quadruple mutant Ant1. These genes may facilitate aggresome formation, a phenotype shared by the cells overexpressing the wild-type and mutant Ant1.

We found that multiple genes involved in RNA processing are up-regulated in cells expressing the mutant Ant1 (Supplemental Figure 5B). These include FUS, RBM12, and SFPQ, which are implicated in amyotrophic lateral sclerosis, frontotemporal dementia, psychosis, and Alzheimer's disease (Kwiatkowski *et al.*, 2009; Vance *et al.*, 2009; Steinberg *et al.*, 2017; Lu *et al.*, 2018; Luisier *et al.*, 2018). Further analysis revealed that 21.7% (*Z*-score = 6.19) and 27.8% (*Z*-score = 25.38) of the total up-regulated genes induced by the triple and quadruple mutants of Ant1 are predicted to be the downstream targets of *EGR1* (Supplemental Tables 5 and 6). More importantly, we found that many genes activated by the mutant Ant1 are involved in cytosolic proteostasis by affecting autophagy, heat shock response, and proteasomal function (Supplemental Figure 5B and Figure 6E). Notably, the up-regulated RAS-related GTP-binding protein, RAB7A, is known to play a

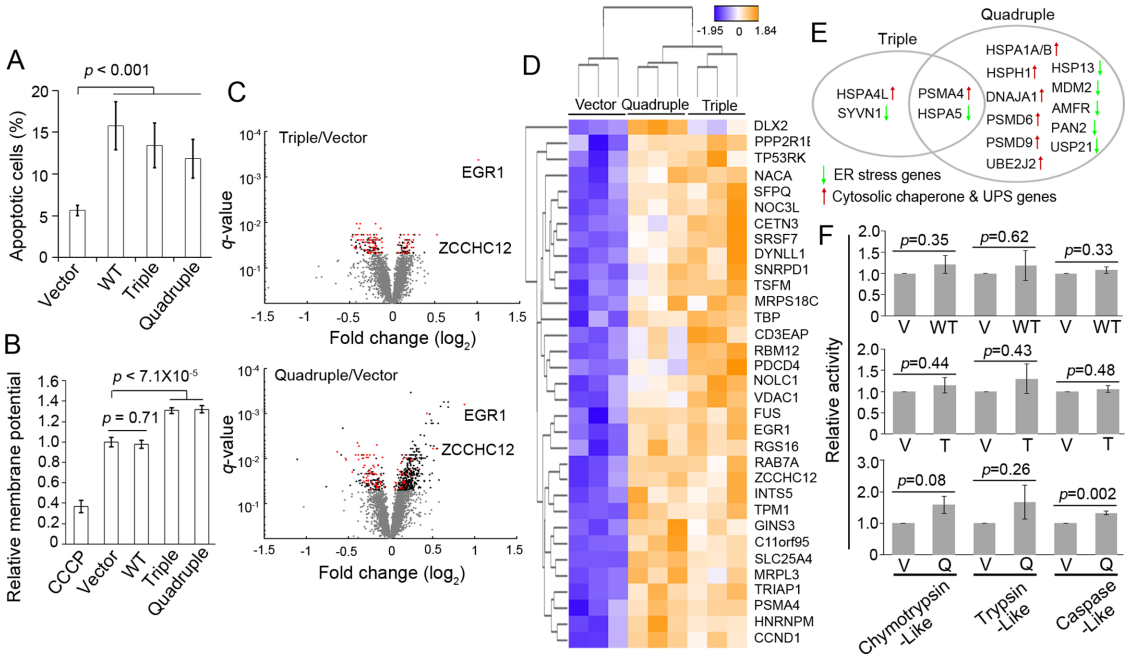

FIGURE 6: Expression of mutant Ant1 triggers proteasomal activation and transcriptional up-regulation of the heat shock response in the cytosol. (A) Apoptosis induced by the expression of mutant versus wild-type Ant1. Depicted here is the percentage of annexin V-positive, PI-negative cells as an indication of early apoptosis from three independent transfections performed in triplicate. Error bars represent SD of three independent experiments in triplicate. (B) Relative mitochondrial membrane potential in the nondepolarized subpopulation of transfected cells (see Supplemental Figure 4 for gating strategy). Error bars represent SEM of three independent experiments in triplicate. (C) Volcano plots showing the distribution of up- and down-regulated genes in HEK293T cells expressing *ant1*^{A90D,L98P,A114P} (triple) and *ant1*^{A90D,L98P,A114P,A123D} (quadruple). (D) Heatmap of the 32 genes that are up-regulated both in cells expressing the triple and quadruple mutants of *ANT1*. Color bar indicates the log2 expression change. (E) Cytosolic proteostatic genes differentially expressed in cells expressing the triple and quadruple mutants of *ANT1*. (F) Relative proteasome-associated proteolytic activities in cells expressing the wild-type (WT), the triple (T), and the quadruple (Q) mutants of *ANT1* compared with vector (V)-transfected cells. Error bars represent SEM of six assays from two independent experiments.

critical role in aggresome formation and maturation (Hyttinen *et al.*, 2014). Genes encoding cytosolic chaperones and the ubiquitin–proteasome system, but not those involved in endoplasmic reticulum stress response, are specifically up-regulated in cells overexpressing the quadruple mutant of Ant1 (Figure 6E). This is consistent with the observation that the caspase-like activity of the proteasome is significantly increased in cells expressing the quadruple but not the triple mutant or wild-type allele of *ANT1* (Figure 6F).

The large number of genes that are transcriptionally remodeled in cells expressing the quadruple mutant of Ant1 allowed us to determine other putative upstream regulators. Ingenuity pathway analysis identified 42 gene clusters predicted to be either activated or inhibited (Supplemental Figure 5C). Genes controlled by ATF4 are up-regulated, supporting the activation of the integrated stress response (Quiros *et al.*, 2017). We found that genes regulated by rapamycin and RICTOR are down-regulated. Rapamycin is an inhibitor of the mechanistic target of rapamycin (mTOR) protein kinase and RICTOR is a subunit of the mTORC2 complex. These observations suggest that expression of the mutant Ant1 down-regulates mTOR signaling, which is known to reduce protein synthesis. This is supported by reduced phosphorylation of 4E-BP and Rps6 (Supplemental Figure 6). Taking the results together, the mutant Ant1 specifically induces multiple branches of proteostatic adaptation in the cytosol, in addition to *EGR1* activation and aggresome formation.

Increased protein ubiquitination, decreased mitochondrial protein solubility, and up-regulated ubiquitin C and eEF1α are common posttranscriptional signatures of cells overexpressing the wild-type and mutant Ant1

As aggresomes are induced by the overexpression of both wild-type and mutant Ant1, we examined posttranscriptional signatures shared by these cells. We hypothesized that aggresomes may contain ubiquitinated misfolded proteins that exhibit reduced solubility. As expected, expression of the wild-type and mutant Ant1 increases protein ubiquitination at virtually all molecular weights in NP-40 insoluble fractions (Figure 7A), suggesting widespread protein misfolding and ubiquitination. The solubility of some mitochondrial proteins (Tom20, Hsp60, and Aco2) is decreased by Ant1 overexpression (Supplemental Figure 7, B, E, and G), but not proteasome inhibition. This observation, together with an aggresome-like distribution of Tom20 and SdhA (Figure 2C), provides strong evidence that carrier-induced aggresomes triage unimported mitochondrial proteins. The detergent solubility of several other mitochondrial proteins (Tim22, SMAC/Diablo, VDAC, and Mia40) is little changed (Supplemental Figure 7, A–D). Furthermore, we found that the cytosolic HSP70 and HSP90 chaperones exhibit reduced solubility in response to proteasome inhibition but not to Ant1 expression (Supplemental Figure 7, F and G). This suggests that these chaperones are either uninvolved or play a minimal role in the triage of unimported mitochondrial proteins via the aggresome pathway.

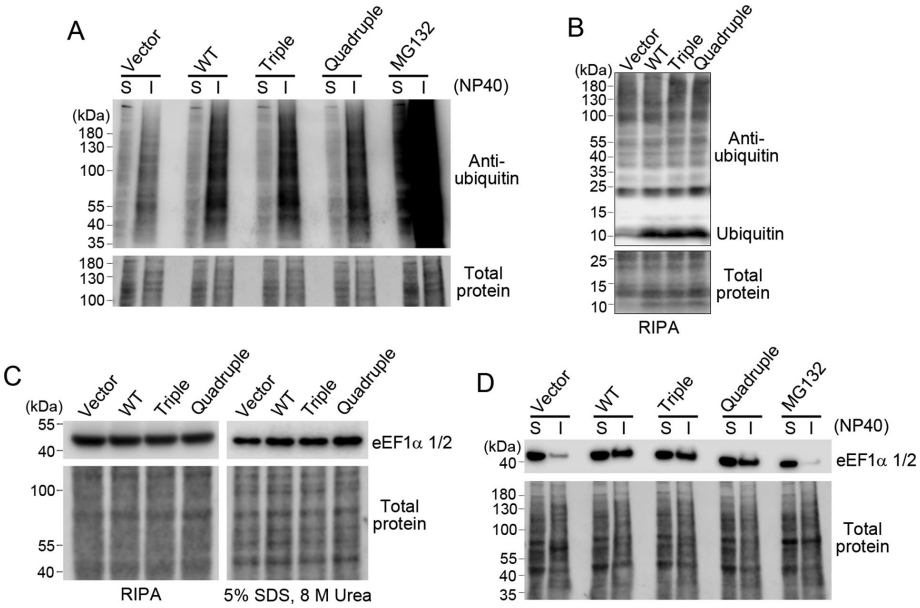

FIGURE 7: Western blot analysis shows increased ubiquitination, free ubiquitin, and eEF1α expression in cells expressing Ant1. (A) Increased ubiquitination in NP-40 insoluble fractions from cells expressing the wild-type and mutant Ant1. (B) Free ubiquitin levels in cells expressing Ant1. (C, D) eEF1α levels in total cell lysate using different detergents (C) and detergent-soluble and -insoluble fractions (D). S, soluble fraction; I, insoluble fraction.

DISCUSSION

In this article, we determined that mPOS can occur in human cells and we identified multiple pathways by which human cells respond to mPOS. We specifically modeled mPOS by overexpressing mitochondrial proteins to see whether proteostatic responses occur in the cytosol when protein loading exceeds import capacity. We found that overexpression of mitochondrial carrier, but not matrix proteins, induces the formation of large aggresomes in the cytosol that contain densely packed protein aggregates. This is accompanied by increased protein ubiquitination and apoptotic cell death, which further support the presence of mPOS in the cytosol. Importantly, we excluded the possibility that mPOS is dependent on accumulation of the overexpressed carrier proteins, as expressing misfolded variants of the carrier protein Ant1 exhibited all signs of mPOS despite a greater than 20-fold reduction in protein accumulation. Therefore, we conclude that saturating the protein import machinery with mitochondrial carrier proteins can impose a drastic proteostatic burden on the cytosol (i.e., mPOS) in human cells.

Although the ratio between LC3-II and LC3-I, a biomarker for autophagy, is significantly increased only in cells expressing the quadruple mutant of Ant1 when proteins are solubilized by RIPA buffer (Supplemental Figure 8A), LC3-II solubility is reduced in all the cells expressing Ant1 (Supplemental Figure 8B). Immunofluorescence microscopy revealed that LC3-positive vesicles are significantly increased in cells expressing mitochondrial carrier but not matrix proteins (Supplemental Figure 8, C and D). These data provide further support for the involvement of the autophagic process in aggresome formation.

Finally, we determined whether processes that are known to stimulate aggresome formation are up-regulated by Ant1 overloading. Recent studies have shown that free ubiquitin serves as signaling molecules to stimulate aggresome processing (Hao *et al.*, 2013). Indeed, we found that the levels of free ubiquitin are increased in cells expressing the wild-type and mutant Ant1 (Figure 7B). Mass spectrometry analysis revealed that the ubiquitin molecules are expressed from the *UBC* (polyubiquitine C) locus (Supplemental Figure 9). In addition, recent studies have shown that the eukaryotic translation elongation factor 1α (eEF1α) forms a CTIF-eEF1A1-DCTN1 complex to facilitate the aggresomal targeting of misfolded polypeptides (Park *et al.*, 2017). We found that the levels of eEF1α in Ant1-overexpressing cells are unchanged in RIPA (1% Triton X-100, 0.1% SDS)-extracted, and slightly increased in SDS/urea (5% SDS, 8 M urea) -extracted cell lysates (Figure 7C). This suggested that eEF1α expression is increased but a fraction of the protein is present in insoluble aggregates. This was confirmed by Western blot showing that eEF1α is heavily enriched in NP-40 insoluble fractions (Figure 7D). Inhibition of proteasome by MG132 does not increase the levels of eEF1α in the NP-40 soluble or insoluble fractions. The data suggest that eEF1α is specifically up-regulated as a stress response to stimulate aggresome formation upon mPOS. As the transcription of *UBC*, *EEF1A1*, and *EEF1A2* are not up-regulated as revealed by RNA-Seq, the increased levels of these proteins must be mediated by posttranscriptional processes.

How do the mutant Ant1 proteins induce aggresomes so robustly while accumulating only to ~5% of the wild-type Ant1 protein level? We speculate that overloading of wild-type and mutant Ant1 similarly saturate the import receptors (e.g., TOM70) and/or cytosolic chaperones that deliver proteins to mitochondria (e.g., HSP70), thereby directly affecting the import efficiency of other mitochondrial proteins. These affected proteins then accumulate in the cytosol and are ultimately transported to the aggresomes. It is likely that the mutant proteins are degraded after the saturated mitochondrial import step, either during translocation through the OMM/IMS or on the IMM. This would explain how the mutant Ant1 proteins effectively induce aggresomes despite such low protein accumulation. However, further experiments are needed to identify the saturated protein import step(s) and the proteolytic pathway(s) responsible for the degradation of the mutant Ant1 proteins.

Our data strongly suggest that mitochondrial carrier-induced aggresomes serve as a mechanism to triage unimported mitochondrial proteins. First, immunofluorescence imaging of aggresome-containing cells showed that endogenous mitochondrial proteins such as Tom20 and SdhA are condensed in vesicle-like structures resembling aggresomes. Second, several endogenous mitochondrial proteins are enriched in detergent-insoluble fractions in cells overexpressing Ant1, which suggests misfolding. There are two likely locations for these misfolded mitochondrial proteins: mitochondria or aggresome. The lack of electron-dense aggregates inside mitochondria on electron micrographs supports an aggresomal localization of the misfolded mitochondrial proteins.

Perhaps not surprisingly, aggresome formation appears to be intimately connected to the autophagy machinery. Double-membrane structures were frequently observed that enclose the aggresomes induced by the mitochondrial carrier Ant1. This suggests that phagophore generation and autophagy are involved in aggresome formation, although membrane structures were not visible in some cases, which may suggest unsealed or even membraneless aggresomes. In support of a phagophore origin of the aggresome-associated

membrane, immunofluorescence revealed that LC3-positive vesicles are significantly increased. Moreover, the most up-regulated gene in response to Ant1 overloading was *EGR1*, which was recently determined to be a transcriptional regulator of autophagy (Peeters *et al.*, 2019). However, it is important to note that the aggresomes are much larger than conventional autophagosomes, and that we have not determined the origin of the aggresomal membrane. It nevertheless remains likely that the aggresomes arise from autophagosomes following continuous aggregate delivery and membrane expansion, or that they are formed by enclosing preexisting protein aggregates with a phagophore membrane.

We also uncovered two likely molecular players in aggresome formation induced by mitochondrial carriers: ubiquitin C and eEF1α1. These two proteins are posttranscriptionally up-regulated. While ubiquitin is well known to participate in general protein turnover, it has also been shown to act as a signaling molecule for the processing of aggresomes (Hao *et al.*, 2013). The eEF1α1 protein, on the other hand, was recently demonstrated to participate in the aggresomal targeting of misfolded cytosolic proteins (Park *et al.*, 2017). These proteins are likely to directly or indirectly participate in the sequestration, trafficking, and processing of unimported mitochondrial proteins. It is important to note that the cytosolic aggresomes are induced in the absence of a severe defect in oxidative phosphorylation and transcriptomic changes that would suggest bioenergetic deficiency and oxidative stress. Aggresome formation is therefore triggered by extramitochondrial proteostatic signals and not, for example, a reduction in ATP levels.

Interestingly, we found that a global inhibition of protein import by MitoBloCK-6 and CCCP, that selectively inhibits the Mia40/Erv1 redox-mediated import pathway and uncouples the IMM, respectively, has either a limited effect or no effect on the induction of aggresomes in the cytosol. We postulate that aggresome formation involves an actively coordinated program that may include aggregate seeding, microtubule organization, intracellular trafficking, phagophore generation, and membrane expansion and sealing. These processes may be dependent on energy homeostasis, cytoskeleton organization, and phospholipid biosynthesis that could be inhibited by MitoBloCK-6 and CCCP-induced mitochondrial damage. Thus, overexpression of the mitochondrial carrier proteins allowed us to capture aggresome formation as a specific response to unbalanced mitochondrial protein loading and import capacity.

Like in yeast (Wang and Chen, 2015), human cells have a limited capacity to tolerate mPOS, and when this capacity is exceeded cells die. However, the specific cell death mechanism induced has not been determined. In this study, apoptosis is induced, but it remains unclear what exactly triggers apoptosis in cells undergoing carrier-induced mPOS. Apoptosis may be induced by extraaggresomal proteostatic stress or by increased release of apoptotic factors from mitochondria. Alternative cell death mechanisms are also possible, particularly autophagic cell death that may occur downstream from the excessive autophagic activity we observed. The mechanism by which mPOS kills cells will be an interesting topic of future work.

As noted above, the data suggest that the import of mitochondrial carriers, which occurs through the TIM22 complex, is saturable. This idea is consistent with a recent study showing that overloading of several noncarrier IMM proteins reduces the import of other TIM23 substrates (Weidberg and Amon, 2018). That study demonstrated an elegant mechanism in yeast, termed mitochondrial compromised protein import response (mitoCPR), which could prevent mPOS induced by saturation of protein import by TIM23 substrates. Our study suggests that aggresomes may form to protect human cells from mPOS induced by saturation of protein import by TIM22 substrates. Under this condition of protein import stress, the transcriptional signature is clearly different from that observed in yeast with activated mitoCPR. It could be that the cellular response to mitochondrial protein import failure is stress and context specific.

Consistent with the above concept, we found that overexpression of mutant Ant1 induces distinct proteostatic stress responses in the cytosol in addition to aggresome formation. Genes involved in protein chaperoning and proteasomal function are up-regulated by the mutant Ant1. These proteostatic adaptations were not observed in cells overexpressing the wild-type Ant1. The Chacinska group has recently demonstrated proteasomal activation in yeast as a response to the inhibition of mitochondrial protein import, which was named unfolded protein response activated by mistargeting of proteins (or UPRam; Wrobel *et al.*, 2015). We speculate that the loading of the misfolded Ant1 may impose a significant intramitochondrial proteolytic burden. This apparently generates a distinct proteostatic signal in the cytosol that activates proteasomal function. The observation that mutant and wild-type Ant1 induce similar levels of apoptotic cell death strongly suggests that Ant1 overloading and misfolding trigger separate rather than additive proteostatic responses, with overloading involving sequestration of aggregates by the aggresomes and misfolding stimulating the proteolytic function of the proteasome. We note that the overexpression of the mutant Ant1 induces both overloading and misfolding, thus aggresome formation and proteasomal activation are both observed.

Clearly, the expression of mitochondrial carrier proteins needs to be tightly controlled in cells, and a balance with the mitochondrial import capacity is important to prevent mPOS. Also important is the folding status of these highly hydrophobic proteins. These are highlighted by many clinical conditions that involve Ant1 overexpression and misfolding. *ANT1* up-regulation is associated with facioscapulohumeral muscular dystrophy (FSHD), dilated cardiomyopathy, and Rett syndrome (Sylven *et al.*, 1993; Dorner *et al.*, 1997; Dorner and Schultheiss, 2000; Laoudj-Chenivesse *et al.*, 2005; Kriaucionis *et al.*, 2006; Forlani *et al.*, 2010). The A90D, L98P, A114P, and A123D alleles of *ANT1* cause dominant pathologies manifested by adPEO, sensorineural hypoacusia, muscle weakness, cardiomyopathy, psychosis, brain atrophy, and dementia (Kaukonen *et al.*, 1999, 2000; Napoli *et al.*, 2001; Siciliano *et al.*, 2003; Deschauer *et al.*, 2005; Palmieri *et al.*, 2005; Liu and Chen, 2013; Simoncini *et al.*, 2017). Thus, our findings could have direct implications for the understanding of these diseases.

The selective induction of proteostatic stress by the mitochondrial carrier proteins could also have implications for the understanding of neuromuscular diseases caused by defects in protein import. This is particularly relevant for the pathway responsible for the import of mitochondrial polytopic membrane proteins (Koehler *et al.*, 1999). Notably, the gene encoding acylglycerol kinase that is mutated in Sengers syndrome has recently been shown to be a subunit of the TIM22 protein translocase complex, which mediates the import and membrane insertion of mitochondrial carrier proteins (Kang *et al.*, 2017; Vukotic *et al.*, 2017). Interestingly, the accumulation of the carrier protein Ant1, which was used extensively in this study, is markedly reduced in Sengers syndrome patients (Jordens *et al.*, 2002; Mayr *et al.*, 2012). One explanation for this observation is that Ant1 import is reduced, and is then degraded in the cytosol in vivo. This would suggest that mPOS could contribute to cell stress in this specific disease in addition to reduced Ant1 activity.

More broadly, mitochondrial proteins are constituents of aggresome-like structures in several common neurodegenerative diseases (e.g., Lewy bodies in Parkinson's disease; Olanow *et al.*, 2004; Power *et al.*, 2017). In light of our study, it would be interesting

to learn whether mPOS contributes to the formation of these aggregates during the initiation or progression of the diseases, especially considering that mitochondrial dysfunction is a prominent hallmark in most neurodegenerative diseases, including Parkinson's.

MATERIALS AND METHODS

Antibodies for Western blot analysis

Antibodies used for Western blot included the Total OXPHOS Human WB Antibody Cocktail (#ab1104a1; Abcam), anti-Aco2 (#ab110321; Abcam), anti-4E-BP1 (#9644; Cell Signaling) and anti-phospho-4E-BP1 (#2855; Cell Signaling), anti-EF-1α1/2 (#sc-377439; Santa Cruz), anti-Hsp60 (#ab59457; Abcam), anti-Hsp70 (#ab47455; Abcam), anti-Hsp90 (#16F1; Enzo), anti-Mdh2 (#sc-293474; Santa Cruz), anti-Mia40 (#sc-365137; Santa Cruz), anti-rpS6 (#ab40820, Abcam); anti-phospho-rpS6 (#ab65748; Abcam), anti-SMAC (#ab8114; Abcam), anti-Tim22 (#14927-1-AP; Proteintech), anti-ubiquitin (#701339; Thermo Scientific), and anti-VDAC (#sc-390996; Santa Cruz). Total proteins were stained with REVERT Total Protein Stain (#926-11011; LI-COR).

Expression of *ANT1* and other genes in HEK293T cells

HEK293T cells were cultured in DMEM (Gibco) supplemented with 10% fetal bovine serum (Sigma) at 37°C in a humidified atmosphere of 5% CO_2. The cDNA of *ANT1* was cloned into the expression vector pCDNA3.1 with a HA epitope added on the C-terminus. The mutant *ANT1* alleles were generated by in vitro mutagenesis using the QuickChange kit (Stratagene). Cells were transfected using Lipofectamine 2000 or 3000 reagent (Invitrogen) with plasmid DNA at a concentration of 0.2 μg/1 × 10^5 seeded cells, and harvested 24 h posttransfection before being used for biochemical analysis and microscopy. pCDNA3.1-based plasmids expressing FLAG-tagged mitochondrial proteins (Slc25A1, Slc25A6, Slc25A11, Aco2, Idh2, and SdhA) were purchased from GenScript. For Western blotting, cells were lysed with RIPA buffer for 30 min and cleared by centrifugation at 16,000 × *g* for 30 min, unless otherwise specified.

Bioenergetic assay

Oxygen consumption rate (OCR) was measured by a Seahorse XF^e 96 Extracellular Flux Analyzer (Agilent Technologies), which employs the oxygen-dependent fluorescence quenching of a fluorophore. HEK293T cells were seeded in the poly-D-lysine–coated microplate at the density of (4.0–6.0) × 10^4 cells/well. The transfection was performed as aforementioned. Before the assay, the transfected cells were washed and incubated in the XF assay medium (Agilent Technologies) supplemented with 10 mM glucose, 1 mM sodium pyruvate, and 2 mM L-glutamine for 1 h at 37°C in an incubator without CO_2. Bioenergetic profiling was obtained by measuring OCR at the basal level, followed by sequential injections of oligomycin (at the final concentration of 2 μM), FCCP (at the final concentration of 0.5 μM), and a mixture of rotenone and antimycin A (at the final concentration of 0.5 μM each). Bioenergetic parameters were calculated from the OCR profile as described in the text.

Aggresome staining and immunostaining

HEK293T and HeLa cells were seeded at approximately 1.75 × 10^5/well in a 24-well plate. Transfection was performed when cells were 60% confluent. Aggresome staining was performed according to the manufacturer's manual (aggresome detection kit; Abcam; #ab139486). Briefly, transfected cells were fixed with 4% formaldehyde and permeabilized by 0.5% Triton X-100 before staining with the aggresome dye and DAPI. Positive control cells were treated with 10 μM MG132 for 24 h. For immunostaining, fixed and permeabilized cells were blocked in phosphate-buffered saline (PBS) containing 3% bovine serum albumin (BSA) followed by anti-HA (#MMS-101R; Covance), anti-FLAG (#PA1-984B; Thermo Fisher Scientific), anti-Tom20 (#42406; Cell Signaling), anti-SdhA (#5839; Cell Signaling), anti-LC3 (#3868; Cell Signaling) antibodies for 1 h at 37°C. After washing with PBST, cells were then incubated with fluorescein-labeled secondary antibody for 45 min at 37°C. Stained cells were visualized using an Image Xpress microconfocal high-content imaging system (Molecular Devices).

Electron microscopy

Cells were harvested 24 h posttransfection, fixed in 2.5% glutaraldehyde at 4°C, and postfixed with 1% osmium tetroxide at room temperature. Cells were then dehydrated, embedded in Luft's Araldite 502 embedding medium (Electron Microscopy Sciences, Hatfield, PA), and cut into thin sections. The ultrathin sections were then stained with uranyl acetate and Reynold's lead citrate (Polysciences). The samples were photographed with a Tecnai BT12 transmission electron microscope (Thermo Fisher Scientific, Hillsboro, OR).

Apoptotic assay

Cells were harvested 24, 36, or 48 h posttransfection and stained for flow cytometry using the FITC Annexin V Apoptosis Detection Kit with PI (BioLegend), per the manufacturer's instructions. A Becton Dickinson Fortessa Cell Analyzer was used to excite dyes with a 488-nm laser. Emission was detected with bandpass filters 610/20 and 530/30 for PI and Annexin V-FITC, respectively. Gating and compensation were performed using cells incubated in 1 μM staurosporine for 24 h as a positive control.

Proteasomal activity assay

HEK293T cells (7 × 10^5) were seeded for transfection. The chymotrypsin-like, trypsin-like, and caspase-like activities were determined 24 h after transfection, using the Proteasome-Glo Assay Systems from Promega (#G8531). Cells were sonicated in PBS plus EDTA (5 mM, pH 7.4) buffer three times for 5 s with 25-s intervals on ice. After the removal of cell debris by centrifugation, the protein concentration of the soluble fractions was determined. Protein samples (10 μg) were used for each assay. Luminescence signals were detected with the SpectraMax i3x Multi-Mode Microplate Reader (Molecular Devices) between 10 and 30 min at room temperature after the addition of luminogenic substrates. The chymotrypsin-like, trypsin-like, and caspase-like activities were calculated by subtracting MG132 (50 μM) -inhibited activities from total activities.

Membrane potential determination

Relative mitochondrial membrane potential was approximated by staining with JC-1 dye (Thermo Fisher Scientific) and measuring fluorescence using flow cytometry according to the manufacturer's instructions. JC-1 exhibits membrane potential-dependent accumulation in mitochondria, indicated by a fluorescence emission shift from green (~529 nm) to red (~590 nm). Reduced red fluorescence was interpreted as a loss of membrane potential. Briefly, 24 h posttransfection in a 12-well plate, HEK293T cells were resuspended in warm medium at ~1 × 10^6 cells/ml and stained with 2 μM JC-1 for 30 min at 37°C and 5% CO_2. For a depolarized control, 100 μM CCCP was added for the incubation. Following incubation, cells were centrifuged at 500 g for 5 min at room temperature, washed once with 1 ml warm PBS, and resuspended in 0.5 ml ice-cold PBS plus 1% BSA for flow cytometry. Samples were excited with a 405-nm laser and emission intensities measured from 525/50 nm (green) and 585/42 nm (red) filters (Becton Dickinson Fortessa Cell Analyzer), as

previously described (Perelman *et al.*, 2012), thus eliminating the need for fluorescence compensation. Data were analyzed using FlowJo v10.0.8.

Submitochondrial protein localization

Submitochondrial fractionation was performed using a protease protection assay. Posttransfection (24 h), full 10-cm plates of HEK293T cells were collected, washed twice with cold PBS, resuspended in 1 ml of cold isotonic buffer (250 mM sucrose, 10 mM Tris-HCl, pH 7.4, 1 mM EDTA, and protease inhibitors), and homogenized on ice with 10 strokes with a 2-ml dounce homogenizer (Pestle clearance 0.0005–0.0025 in.). Unbroken cells and nuclei were cleared by centrifugation at 600 × *g* for 15 min at 4°C, and postnuclear supernatant was centrifuged at 10,000 × *g* for 25 min at 4°C to pellet mitochondria. The mitochondrial pellet was resuspended in 100 µl isotonic buffer with protease inhibitors. Three 10-cm plates worth of mitochondria were combined to increase yield (only 60 mg of mitochondria per plate), and protein concentration was determined using a Bradford assay. Mitochondria were then distributed into 30-µg aliquots and pelleted again, as above. Pellets were resuspended in 16–20 µl of either isotonic or hypotonic buffer (10 mM KCl, 2 mM HEPES, pH 7.2) without protease inhibitors. To burst the mitochondrial outer membrane, hypotonic resuspensions were incubated on ice for 20 min. To lyse the mitochondrial inner membrane, Triton X-100 was added for a final concentration of 1%, and samples were incubated on ice for 10 mins. To degrade accessible proteins, Proteinase K was then added for a final concentration of 7 µg/ml and incubated at room temperature for 20 min. Proteinase K digestion was stopped with 5 mM phenylmethylsulfonyl fluoride (PMSF) and 15 mins on ice. Laemmli buffer was added to all samples for SDS–PAGE, and 15 µg of protein was loaded in each lane.

Cellular fractionation

Transfected HEK293T cells were fractionated into soluble and insoluble fractions using two different lysis buffers: NP-40 buffer (1% NP40, 10 mM Tris-HCl, pH 7.4, 5 mM EDTA, 150 mM NaCl) for soluble proteins and Triton buffer (PBS with 1% Triton X-100) for membrane proteins. Posttransfection (24 h), cells from a six-well plate were collected, washed once with cold PBS, lysed with 50 µl cold lysis buffer supplemented with protease inhibitors, and incubated on ice for 20 min. Lysates separated into soluble and insoluble fractions by centrifugation at 16,000 × *g* for 30 min. Supernatant was collected as the soluble fraction, protein concentration was determined using Bradford assay, and samples were mixed with 3× Laemmli buffer to load 25 µg protein per sample. The insoluble pellet was washed with 50 µl of either NP-40 buffer or Triton buffer. The insoluble pellet was then solubilized by resuspension in 100 µl of sample buffer (5% SDS, 8 M urea, 40 mM Tris-HCl, pH 6.8, 0.1 mM EDTA, 1% β-mercaptoethanol, and 0.01% bromophenol blue) followed by sonication. Each sample (10 µl per sample, 10% of insoluble fraction) was then loaded onto a polyacrylamide gel for SDS–PAGE and Western blotting.

For silver-stained gels, each lane contained the entire NP-40–soluble fraction from one well of a six-well plate. Samples were mixed with 3× Laemmli buffer and solubilized for 1 h at 42°C. The gel was stained as previously described (Shevchenko *et al.*, 1996). Briefly, the gel was fixed in 50% methanol, 5% acetic acid for 20 min, washed in 50% methanol for 10 min, and then washed overnight in water. The next day the gel was sensitized in 0.02% anhydrous $Na_2S_2O_3$ for 1 min, washed twice in water for 1 min each, stained in 0.1% $AgNO_3$ for 20 min, washed two more times in water for 1 min, and developed in 0.04% Formalin, 2% Na_2CO_3 for ~10 min, and staining was terminated in 5% acetic acid.

Mass spectrometry

Protein identification in bands of silver-stained gels was performed using mass spectrometry after in-gel trypsinization. Liquid chromatography (LC)–MS analysis was performed using a Waters nanoAcquity LC and autosampler coupled to an Orbitrap XL hybrid ion trap Orbitrap mass spectrometer, operated in a top-five data-dependent mode using survey scans at 30,000 resolution from 375 to 1800 m/z. Tandem MS scans were acquired in the ion trap with an isolation width of 2 m/z and fragmentation mode was CID with 35% normalized collision energy for 0.1 ms. The automatic gain control settings were 3×10^5 ions in the ion trap, and 1×10^6 in the Orbitrap. Dynamic exclusion was used with a duration of 15 s and a repeat count of 1. Tandem mass spectra were searched against a human database, with common contaminant proteins using the Sequest HT node in Proteome Discoverer 1.4. Search parameters included variable modifications of methionine oxidation, partial trypsin specificity with two missed cleavages allowed. Search results were filtered to Percolator *q* values < 0.01 and peptide confidence filter set for "high."

Detergent extraction of misfolded Ant1

We extracted the wild-type and quadruple mutant Ant1 from transfected cells using a battery of lysis buffers (i.e., detergents and detergent combinations). Lysis buffers were diluted in 20 mM Tris-HCl (pH 7.4) and included RIPA buffer (20 mM Tris-HCl, pH 7.4, 150 mM NaCl, 1 mM EDTA, 1% Triton X-100, 0.1% SDS, with freshly added PMSF to 1 mM and protease inhibitors); 8 M guanidine-HCl; 2% sarkosyl; 2% sarkosyl plus 0.1% LPPG (1-palmitoyl-2-hydroxy-d31-sn-glycero-3-phosphoglycerol); 2% SDS; 4% SDS; 4% SDS plus 7 M urea plus 2 M thiourea plus 4% CHAPS (3-((3-cholamidopropyl) dimethylammonio)-1-propanesulfonate); 5% SDS plus 8 M urea; 5% SDS plus 8 M urea plus 2% Triton X-100; and 5% SDS plus 8M urea plus 2% sarkosyl. The same general protocol was used for all lysis buffers except guanidine. This general protocol was as follows: transfected cells were collected from their 12-well plate and washed twice with cold PBS, followed by cell lysis with 50 µl lysis buffer. The lysate was then sonicated and incubated at room temperature or on ice (for the RIPA samples only) for 1 h. Lysates were then cleared by centrifugation at 16,000 × *g* for 20 min, and 10% of the supernatant was loaded onto a polyacrylamide for each sample. The guanidine sample required extra steps after lysis due to the incompatibility of guanidine-containing samples and SDS–PAGE. Guanidine lysates were incubated at 25°C for 1 h and similarly sonicated and centrifuged at 16,000 × *g* for 20 min at room temperature. Protein was precipitated from the supernatant by adding nine volumes of –20°C 100% ethanol and incubating overnight at –20°C. This was then centrifuged at 16,000 × *g* for 15 min, the pellet was washed with –20°C 90% ethanol, and dried samples were resuspended in sample buffer (5% SDS, 8 M urea, 40 mM Tris-HCl, pH 6.8, 0.1 mM EDTA, 1% β-mercaptoethanol, and 0.01% bromophenol blue). As for the other samples, 10% of the sample was loaded onto a polyacrylamide gel.

RNA-Seq analysis

Total RNA was extracted from transfected HEK293T cells using a RNeasy mini kit (Qiagen). The quality of total RNA was validated by Bioanalyzer (Agilent Technologies). Approximately 1 µg of RNA per sample was used to construct the cDNA library using a TruSeq stranded mRNA library prep kit (Illumina), followed by quantitation

using a KAPA library quantification kit for Illumina platforms (Kapa Biosystems). The individual indexed libraries were diluted to 4 nM and pooled in equal quantity, then denatured before loading onto the Illumina NextSeq 500. The sequencing was run as paired-end reads (2 × 75 base pairs per read) with a targeted depth of 60 million paired-end reads per sample. Three independent replicates were performed for each sample. Reads were aligned to GRCh37/hg19 using TopHat (v1.1.0). PartekFlow (Partek, St. Louis, MO) was used for quantification and normalization with the reads per kilobase per million mapped reads method. The gene-specific analysis (GSA) statistical method was used to analyze the differential expression with default settings. The GSA algorithm fits the observed data for each gene to different statistical distributions (e.g., normal, log-normal, negative-binomial, Poisson) and assesses the evidence for differential expressed for the model with the best goodness of fit (as determined by the Akaike information criterion). The genes with q value < 0.05 were considered as differentially expressed genes. The analysis of top canonical pathways and upstream regulators was performed using ingenuity pathway analysis (Qiagen).

Transcription factor analysis

We searched for overrepresented transcription factor binding sites in the 2 kb upstream region of genes significantly up-regulated by overexpression of wild-type or mutant *ANT1* alleles using oPOSSUM version 3.0.

Statistical analysis, data deposition, and availability

Two-tailed Student's t tests were used to calculate the p values. All raw FastQ files and normalized expression data from the RNA-Seq experiments have been deposited into the NCBI Gene Expression Omnibus/Sequence Read Archive (accession number: GSE108622). The data that support the findings of this study are available from the corresponding author upon reasonable request.

ACKNOWLEDGMENTS

We thank Yu Chen, the Kotula lab, and Ebbing de Jong for help in graphic preparation, confocal microscopy, and mass spectrometry, respectively. This work was supported by National Institutes of Health (NIH) Grants no. AG-023731 and no. AG-061204 to X.J.C. and predoctoral fellowships from the American Heart Association (13PRE16820055) and NIH (F30AG-060702) to Y.L. and L.P.C., respectively.

REFERENCES

Calvo SE, Clauser KR, Mootha VK (2016). MitoCarta2.0: an updated inventory of mammalian mitochondrial proteins. Nucleic Acids Res 44, D1251–D1257.

Chacinska A, Koehler CM, Milenkovic D, Lithgow T, Pfanner N (2009). Importing mitochondrial proteins: machineries and mechanisms. Cell 138, 628–644.

Coyne LP, Chen XJ (2018). mPOS is a novel mitochondrial trigger of cell death—implications for neurodegeneration. FEBS Lett 592, 759–775.

Dabir DV, Hasson SA, Setoguchi K, Johnson ME, Wongkongkathep P, Douglas CJ, Zimmerman J, Damoiseaux R, Teitell MA, Koehler CM (2013). A small molecule inhibitor of redox-regulated protein translocation into mitochondria. Dev Cell 25, 81–92.

Deschauer M, Hudson G, Muller T, Taylor RW, Chinnery PF, Zierz S (2005). A novel ANT1 gene mutation with probable germline mosaicism in autosomal dominant progressive external ophthalmoplegia. Neuromuscul Disord 15, 311–315.

Dorner A, Schultheiss HP (2000). The myocardial expression of the adenine nucleotide translocator isoforms is specifically altered in dilated cardiomyopathy. Herz 25, 176–180.

Dorner A, Schulze K, Rauch U, Schultheiss HP (1997). Adenine nucleotide translocator in dilated cardiomyopathy: pathophysiological alterations in expression and function. Mol Cell Biochem 174, 261–269.

Forlani G, Giarda E, Ala U, Di Cunto F, Salani M, Tupler R, Kilstrup-Nielsen C, Landsberger N (2010). The MeCP2/YY1 interaction regulates ANT1 expression at 4q35: novel hints for Rett syndrome pathogenesis. Hum Mol Genet 19, 3114–3123.

Gabellini D, Green MR, Tupler R (2002). Inappropriate gene activation in FSHD: a repressor complex binds a chromosomal repeat deleted in dystrophic muscle. Cell 110, 339–348.

Garcia-Mata R, Bebok Z, Sorscher EJ, Sztul ES (1999). Characterization and dynamics of aggresome formation by a cytosolic GFP-chimera. J Cell Biol 146, 1239–1254.

Gottschling DE, Nystrom T (2017). The upsides and downsides of organelle interconnectivity. Cell 169, 24–34.

Hao R, Nanduri P, Rao Y, Panichelli RS, Ito A, Yoshida M, Yao TP (2013). Proteasomes activate aggresome disassembly and clearance by producing unanchored ubiquitin chains. Mol Cell 51, 819–828.

Hyttinen JM, Amadio M, Viiri J, Pascale A, Salminen A, Kaarniranta K (2014). Clearance of misfolded and aggregated proteins by aggrephagy and implications for aggregation diseases. Ageing Res Rev 18, 16–28.

Jordens EZ, Palmieri L, Huizing M, van den Heuvel LP, Sengers RC, Dorner A, Ruitenbeek W, Trijbels FJ, Valsson J, Sigfusson, *et al*. (2002). Adenine nucleotide translocator 1 deficiency associated with Sengers syndrome. Ann Neurol 52, 95–99.

Kang Y, Stroud DA, Baker MJ, De Souza DP, Frazier AE, Liem M, Tull D, Mathivanan S, McConville MJ, Thorburn DR, *et al*. (2017). Sengers syndrome-associated mitochondrial acylglycerol kinase is a subunit of the human TIM22 protein import complex. Mol Cell 67, 457–470 e455.

Kaukonen J, Juselius JK, Tiranti V, Kyttala A, Zeviani M, Comi GP, Keranen S, Peltonen L, Suomalainen A (2000). Role of adenine nucleotide translocator 1 in mtDNA maintenance. Science 289, 782–785.

Kaukonen J, Zeviani M, Comi GP, Piscaglia MG, Peltonen L, Suomalainen A (1999). A third locus predisposing to multiple deletions of mtDNA in autosomal dominant progressive external ophthalmoplegia. Am J Hum Genet 65, 256–261.

Koehler CM, Leuenberger D, Merchant S, Renold A, Junne T, Schatz G (1999). Human deafness dystonia syndrome is a mitochondrial disease. Proc Natl Acad Sci USA 96, 2141–2146.

Kolodziejska KE, Burns AR, Moore RH, Stenoien DL, Eissa NT (2005). Regulation of inducible nitric oxide synthase by aggresome formation. Proc Natl Acad Sci USA 102, 4854–4859.

Kopito RR (2000). Aggresomes, inclusion bodies and protein aggregation. Trends Cell Biol 10, 524–530.

Kriaucionis S, Paterson A, Curtis J, Guy J, Macleod N, Bird A (2006). Gene expression analysis exposes mitochondrial abnormalities in a mouse model of Rett syndrome. Mol Cell Biol 26, 5033–5042.

Kwiatkowski TJ Jr, Bosco DA, Leclerc AL, Tamrazian E, Vanderburg CR, Russ C, Davis A, Gilchrist J, Kasarskis EJ, Munsat, *et al*. (2009). Mutations in the FUS/TLS gene on chromosome 16 cause familial amyotrophic lateral sclerosis. Science 323, 1205–1208.

Laoudj-Chenivesse D, Carnac G, Bisbal C, Hugon G, Bouillot S, Desnuelle C, Vassetzky Y, Fernandez A (2005). Increased levels of adenine nucleotide translocator 1 protein and response to oxidative stress are early events in facioscapulohumeral muscular dystrophy muscle. J Mol Med 83, 216–224.

Liu W, Duan X, Fang X, Shang W, Tong C (2018). Mitochondrial protein import regulates cytosolic protein homeostasis and neuronal integrity. Autophagy 14, 1293–1309.

Liu Y, Chen XJ (2013). Adenine nucleotide translocase, mitochondrial stress, and degenerative cell death. Oxid Med Cell Longev 2013, 146860.

Liu Y, Wang X, Chen XJ (2015). Misfolding of mutant adenine nucleotide translocase in yeast supports a novel mechanism of Ant1-induced muscle diseases. Mol Biol Cell 26, 1985–1994.

Lu J, Shu R, Zhu Y (2018). Dysregulation and dislocation of SFPQ disturbed DNA organization in Alzheimer's disease and frontotemporal dementia. J Alzheimers Dis 61, 1311–1321.

Luisier R, Tyzack GE, Hall CE, Mitchell JS, Devine H, Taha DM, Malik B, Meyer I, Greensmith L, Newcombe J, *et al*. (2018). Intron retention and nuclear loss of SFPQ are molecular hallmarks of ALS. Nat Commun 9, 2010.

Mayr JA, Haack TB, Graf E, Zimmermann FA, Wieland T, Haberberger B, Superti-Furga A, Kirschner J, Steinmann B, Baumgartner MR, *et al*. (2012). Lack of the mitochondrial protein acylglycerol kinase causes Sengers syndrome. Am J Hum Genet 90, 314–320.

Napoli L, Bordoni A, Zeviani M, Hadjigeorgiou GM, Sciacco M, Tiranti V, Terentiou A, Moggio M, Papadimitriou A, Scarlato G, Comi GP (2001). A novel missense adenine nucleotide translocator-1 gene mutation in a Greek adPEO family. Neurology 57, 2295–2298.

Ogunbona OB, Baile MG, Claypool SM (2018). Cardiomyopathy-associated mutation in the ADP/ATP carrier reveals translation-dependent regulation of cytochrome *c* oxidase activity. Mol Biol Cell 29, 1449–1464.

Olanow CW, Perl DP, DeMartino GN, McNaught KS (2004). Lewy-body formation is an aggresome-related process: a hypothesis. Lancet Neurol 3, 496–503.

Palmieri L, Alberio S, Pisano I, Lodi T, Meznaric-Petrusa M, Zidar J, Santoro A, Scarcia P, Fontanesi F, Lamantea E, *et al*. (2005). Complete loss-of-function of the heart/muscle-specific adenine nucleotide translocator is associated with mitochondrial myopathy and cardiomyopathy. Hum Mol Genet 14, 3079–3088.

Park J, Park Y, Ryu I, Choi MH, Lee HJ, Oh N, Kim K, Kim KM, Choe J, Lee C, *et al*. (2017). Misfolded polypeptides are selectively recognized and transported toward aggresomes by a CED complex. Nat Commun 8, 15730.

Peeters JGC, Picavet LW, Coenen S, Mauthe M, Vervoort SJ, Mocholi E, de Heus C, Klumperman J, Vastert SJ, Reggiori F, *et al*. (2019). Transcriptional and epigenetic profiling of nutrient-deprived cells to identify novel regulators of autophagy. Autophagy 15, 98–112.

Perelman A, Wachtel C, Cohen M, Haupt S, Shapiro H, Tzur A (2012). JC-1: alternative excitation wavelengths facilitate mitochondrial membrane potential cytometry. Cell Death Dis 3, e430.

Power JH, Barnes OL, Chegini F (2017). Lewy bodies and the mechanisms of neuronal cell death in Parkinson's disease and dementia with Lewy bodies. Brain Pathol 27, 3–12.

Quiros PM, Prado MA, Zamboni N, D'Amico D, Williams RW, Finley D, Gygi SP, Auwerx J (2017). Multi-omics analysis identifies ATF4 as a key regulator of the mitochondrial stress response in mammals. J Cell Biol 216, 2027–2045.

Richter-Dennerlein R, Oeljeklaus S, Lorenzi I, Ronsor C, Bareth B, Schendzielorz AB, Wang C, Warscheid B, Rehling P, Dennerlein S (2016). Mitochondrial protein synthesis adapts to influx of nuclear-encoded protein. Cell 167, 471–483.e410.

Ruprecht JJ, Hellawell AM, Harding M, Crichton PG, McCoy AJ, Kunji ER (2014). Structures of yeast mitochondrial ADP/ATP carriers support a domain-based alternating-access transport mechanism. Proc Natl Acad Sci USA 111, E426–E434.

Shadel GS, Horvath TL (2015). Mitochondrial ROS signaling in organismal homeostasis. Cell 163, 560–569.

Shevchenko A, Wilm M, Vorm O, Mann M (1996). Mass spectrometric sequencing of proteins silver-stained polyacrylamide gels. Anal Chem 68, 850–858.

Siciliano G, Tessa A, Petrini S, Mancuso M, Bruno C, Grieco GS, Malandrini A, DeFlorio L, Martini B, Federico A, *et al*. (2003). Autosomal dominant external ophthalmoplegia and bipolar affective disorder associated with a mutation in the ANT1 gene. Neuromuscul Disord 13, 162–165.

Simoncini C, Siciliano G, Tognoni G, Mancuso M (2017). Mitochondrial ANT-1 related adPEO leading to cognitive impairment: is there a link? Acta Myol 36, 25–27.

Steinberg S, Gudmundsdottir S, Sveinbjornsson G, Suvisaari J, Paunio T, Torniainen-Holm M, Frigge ML, Jonsdottir GA, Huttenlocher J, Arnarsdottir S, *et al*. (2017). Truncating mutations in RBM12 are associated with psychosis. Nat Genet 49, 1251–1254.

Sylven C, Lin L, Jansson E, Sotonyi P, Fu LX, Waagstein F, Hjalmarsson A, Marcus C, Bronnegard M (1993). Ventricular adenine nucleotide translocator mRNA is upregulated in dilated cardiomyopathy. Cardiovasc Res 27, 1295–1299.

Vance C, Rogelj B, Hortobagyi T, De Vos KJ, Nishimura AL, Sreedharan J, Hu X, Smith B, Ruddy D, Wright P, *et al*. (2009). Mutations in FUS, an RNA processing protein, cause familial amyotrophic lateral sclerosis type 6. Science 323, 1208–1211.

Vukotic M, Nolte H, Konig T, Saita S, Ananjew M, Kruger M, Tatsuta T, Langer T (2017). Acylglycerol kinase mutated in Sengers syndrome is a subunit of the TIM22 protein translocase in mitochondria. Mol Cell 67, 471–483.e477.

Wang X (2001). The expanding role of mitochondria in apoptosis. Genes Dev 15, 2922–2933.

Wang X, Chen XJ (2015). A cytosolic network suppressing mitochondria-mediated proteostatic stress and cell death. Nature 524, 481–484.

Weidberg H, Amon A (2018). MitoCPR-A surveillance pathway that protects mitochondria in response to protein import stress. Science 360, eaan4146.

Wrobel L, Topf U, Bragoszewski P, Wiese S, Sztolsztener ME, Oeljeklaus S, Varabyova A, Lirski M, Chroscicki P, Mroczek S, *et al*. (2015). Mistargeted mitochondrial proteins activate a proteostatic response in the cytosol. Nature 524, 485–488.